Sensors & Actuators: A. Physical 362 (2023) 114667

Contents lists available at ScienceDirect

Sensors and Actuators: A. Physical

journal homepage: www.journals.elsevier.com/sensors-and-actuators-a-physical

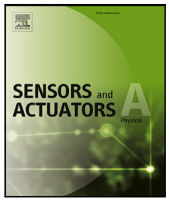

Nonlinear phenomena in magnetic plucking of piezoelectric vibration energy harvesters

Michele Rosso [a,*], Eetu Kohtanen [b], Alberto Corigliano [a], Raffaele Ardito [a], Alper Erturk [b]

[a] Department of Civil and Environmental Engineering, Politecnico di Milano, Piazza Leonardo da Vinci 32, Milano, 20133, Italy
[b] G.W. Woodruff School of Mechanical Engineering, Georgia Institute of Technology, 771 Ferst Dr NW, Atlanta, 30332, GA, United States of America

ARTICLE INFO

Keywords:
Piezoelectric energy harvesting
Magnetic plucking
Nonlinear dynamics
Frequency up-conversion

ABSTRACT

This work presents an investigation on the dynamics of a magnetically frequency up-converted piezoelectric energy harvester. The magnetic interaction arises between a tip magnet on a piezoelectric bimorph and a moving magnet. The latter is controlled through a low-frequency shaker at a fixed frequency of 3 Hz. We investigate in detail the effect of increasing velocity interaction between the magnets at the same input frequency, in terms of frequency up-conversion (i.e. migration from slow to fast dynamics). We show that, for increasing velocity of interaction, the frequency of the first bending mode of the piezoelectric bimorph gradually appears. Also material nonlinearities are observed as a frequency shift of the bending mode. The work shows also that the magnetic plucking phenomenon can be reliably simulated by means of a reduced order model that takes into account material nonlinearities.

1. Introduction

The growing need to create an interconnected world through smart devices makes autonomous sensing an attractive goal, with the aim of reducing the use of batteries. Among energy harvesting and transduction mechanisms, the exploitation of the kinetic energy from environmental vibrations using structures equipped with piezoelectric material is one of the most promising [1,2]. In this way, it is possible to convert mechanical energy into electrical by the so-called direct piezoelectric effect [3,4], whereas the inverse effect is adopted for actuation purposes [5]. The research in this field initially focused on the transduction mechanism for linear systems [6–8]. Unfortunately, these studies have shown that without a strong dynamic amplification of piezoelectric transducers (i.e. near resonance condition), only low amounts of energy can be recovered [9]. The excitation at resonance is difficult to obtain, since the transducers are typically small objects characterized by relatively high resonance frequencies (i.e. hundreds or even thousands of hertz) while ambient vibration has a strong energy density below one hundred hertz [6].

To solve this limitation, frequency up-conversion techniques were introduced through plucking mechanisms. Some of these make use of mechanical contact through plectra [10,11], others are realized through impacts [12,13], or through magnetic interaction between permanent magnets. The latter technique is favorable as it avoids impacts and early degradation of the piezoelectric crystals [14]. Magnetic plucking was initially introduced by considering two separate but coupled oscillating systems. Typically, a transducer equipped with a magnet vibrates due to the interaction provided by another magnet mounted on a dynamic system able to vibrate at low frequency. In such a way it is possible to create an impulsive force directly applied to the energy harvester [15–17]. Many systems in the literature are based on a rotational mechanism, such as Pillatsch et al. [18,19], Fu and Yeatman [20], and Shu et al. [21], who also recently exploited the activation of different structural modes [22]. Studies on the best orientation of the magnets on these rotational mechanisms have been made by Xue and Roundy [23]. The aforementioned studies are conducted by considering the input driving frequency, in the range of 1–35 Hz as a parameter for the harvester performance. The literature lacks a specific study on the effect of the magnetic interaction velocity on the magnetic FuC. To the best of our knowledge, the only study about the velocity was carried out by Dauksevicius et al. [24] without considering the nature of the material response (i.e. linear or nonlinear), with reference to rotational mechanisms. Moreover, the relative velocities that are considered in that paper are by far larger than the typical values of human motion.

In this work, we first investigate in detail the effect of increasing velocity interaction between the moving magnets at the same input frequency, in terms of frequency up-conversion (i.e. migration from slow to fast dynamics). Then, we observe and discuss inherent piezoelectric

* Corresponding author.
E-mail addresses: michele.rosso@polimi.it (M. Rosso), ekohtanen3@gatech.edu (E. Kohtanen), alberto.corigliano@polimi.it (A. Corigliano), raffaele.ardito@polimi.it (R. Ardito), alper.erturk@me.gatech.edu (A. Erturk).

https://doi.org/10.1016/j.sna.2023.114667
Received 27 July 2023; Received in revised form 1 September 2023; Accepted 17 September 2023
Available online 20 September 2023

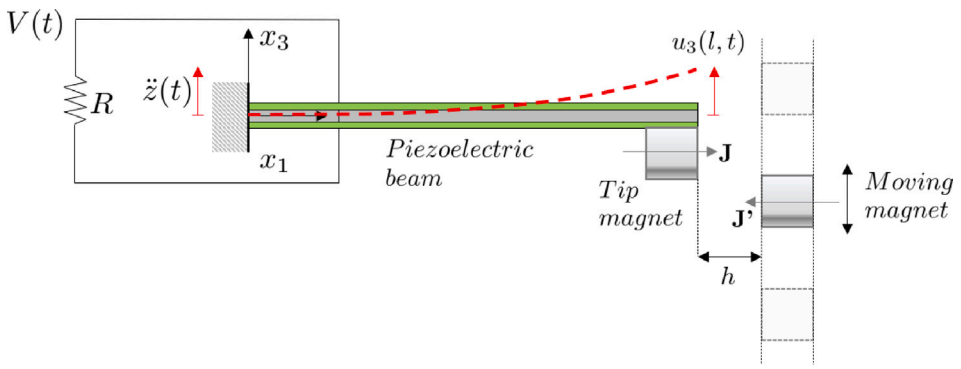

Fig. 1. Schematic of the typical bimorph for energy harvesting with piezoelectric layers in series connection with addition of the magnets for the magnetic plucking.

(material) nonlinearities that may arise during the magnetic plucking, and their implications in terms of energy harvesting.

The paper is organized as follows: Section 2 presents the modeling for the piezoelectric energy harvester and the magnetic force, together with the calibration of the mathematical model parameters. Section 3 presents the experimental investigation and the comparison with the numerical time domain simulation and the discussion of the results. Various effects of the system response are analyzed: velocity of interaction between magnets, gap distance, and electrical load resistance. Closing remarks are provided in Section 4.

2. Modeling

2.1. Piezoelectric bimorph model

To describe the behavior of the piezoelectric transducer, the unified nonlinear nonconservative electroelastic model proposed in [25] is adopted. The model is valid under moderately high mechanical and electrical excitation levels. Both hysteretic elastic and electromechanical nonlinear coupling are considered. The ferroelectric hysteresis is not considered since it is assumed that the piezoelectric layers work well below the coercive field, as will be shown later. The following expression of nonlinear enthalpy density H_p is assumed for the piezoelectric material [25]:

$$H_p = \frac{1}{2}c_{11,p}S_1^2+\frac{1}{3}c_{111,p}S_1^3\,\mathrm{sgn}(S_1)-e_{31}S_1E_3-\frac{1}{2}e_{311}S_1^2\,\mathrm{sgn}(S_1)E_3-\frac{1}{2}\varepsilon_{33}E_3^2 \tag{1}$$

where S_1 is the axial strain, E_3 is the electric field in the polarization direction, $c_{11,p}$ and e_{31} are the linear elastic and piezoelectric constants, and $c_{111,p}$ and e_{311} are the nonlinear elastic and piezoelectric constants. ε_{33} is the dielectric constant. The nonconservative work is assumed as in [25], which takes into account the first and second order structural damping and the Joule heating of the load resistance (see Appendix A).

In Eq. (1), the presence of the sign function states that the enthalpy density is expressed in the strain amplitude rather than the strain itself. In this way, the second-order terms do not disappear, in the equation of motion, if the model is applied to a symmetric layering. Such a choice is justified by the fact that if third-order nonlinearities are introduced to avoid the effect of vanishing second-order terms, an experimental inconsistency in terms of backbone curves is observed. In fact, the model also predicts a linear backbone curve in the range where nonlinearity is pronounced, which was experimentally demonstrated [25,26]. The piezoelectric cantilever beam with a tip mass is modeled by adopting the Euler–Bernoulli structural theory. A schematic of the beam, together with the moving magnet in typical positions that will be adopted in the experiment, is shown in Fig. 1.

The stresses T_1 and the electric displacement D_3 are computed through the equations:

$$T_1 = \frac{\partial H_p}{\partial S_1} \tag{2}$$

$$D_3 = -\frac{\partial H_p}{\partial E_3} \tag{3}$$

To spatially discretize the problem, Galerkin's method is applied by using only one degree-of-freedom (dof) $u(t)$ for the transversal displacements of the beam $u_3(x_1,t)$ and voltage at the electrodes $v(t)$ (see Appendix A). By applying Hamilton's principle, the electromechanical equations of motions are represented by the following system of ordinary differential equations (ODEs, see Appendix A for details):

$$\begin{cases} m\ddot{u} + \left[b_1 u\,\mathrm{sgn}(u) + b_2u^2\right]\mathrm{sgn}(\dot{u}) + k_1u + k_2u^2\,\mathrm{sgn}(u) + \\ -\left[\theta_1 + \theta_2 u\,\mathrm{sgn}(u)\right]v = f_{ext} \\ C\dot{v} + \frac{v}{R} + \left[\theta_1 + \theta_2 u\,\mathrm{sgn}(u)\right]\dot{u} = 0 \end{cases} \tag{4}$$

where f_{ext} represents the sum of all external forces acting on the mechanical dof. m is the modal mass of the first mode, b_1, k_1 θ_1 are the linear damping, stiffness, and coupling coefficients respectively, while b_2, k_2, and θ_2 are the nonlinear counterparts. C is the effective capacitance of the piezoelectric cantilever.

2.2. Magnetic force

The investigation on the modeling of the magnetic forces has been conducted in a previous work [16]. To avoid cumbersome finite element analysis (FEA), the analytical formula provided by Akoun and Yonnet in [27] is adopted, which supposes uniform and rigid magnetization of the involved magnets. It is in good agreement with FEA results and experiments.

The interacting magnets are represented in Fig. 2. If i is the cartesian direction of the force component in which one is interested in, the force is computed with the formula:

$$F_i = \frac{\mathbf{J}\cdot\mathbf{J}'}{4\pi\mu_0}\sum_{m=0}^{1}\sum_{n=0}^{1}\sum_{p=0}^{1}\sum_{q=0}^{1}\sum_{r=0}^{1}\sum_{s=0}^{1}(-1)^{m+n+p+q+r+s}\phi_i(U_{mn},V_{pq},W_{rs},R) \tag{5}$$

where $\mathbf{J}$ and $\mathbf{J}'$ are the magnetization vectors (in Tesla) and μ_0 is the in-vacuum magnetic permeability equal to $4\pi10^{-7}$ H/m. The parameters m,n,p,q,r,s can be equal to 1 or 0 and their combination identifies the corner of the magnets. The coefficients ϕ_i depend on the geometrical dimensions of the magnets. For details on ϕ_i, U_{mn}, V_{pq}, W_{rs}, R, see Appendix B. In the experiments the magnets are cubic NdFeB with a side length of 3.18 mm and a magnetization of 1.32 T (K&J Magnetics, Inc. B222).

2.3. Model calibration

Except for the mechanical damping, all the linear parameters in the differential system (4) can be computed from supplier data. On the other hand, the identification of nonlinear parameters requires experimentation [25,28]. To identify the linear damping coefficient

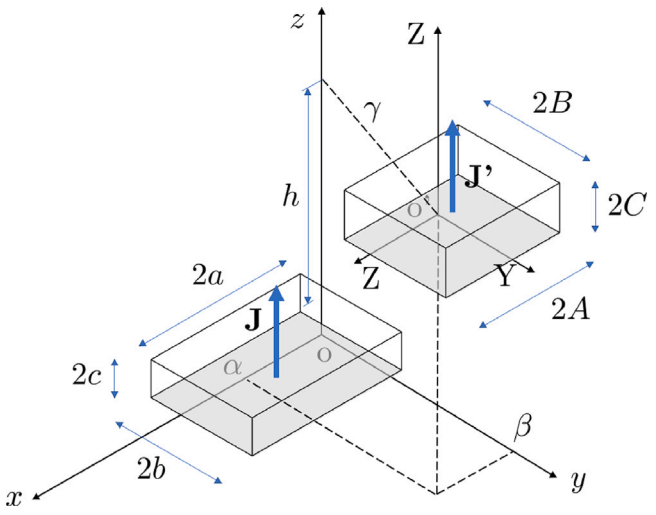

Fig. 2. Illustration of a couple of interacting permanent magnets implemented from [27].

b_1, and the nonlinear parameters $c_{111,p}$, e_{311}, and b_2 a Piezo Systems Inc. brass-reinforced T226-A4-103X bimorph beam with PZT-5A active material and equipped with a tip magnet is employed in a base-excitation setup featuring a Brüel and Kjær Type 4809 electrodynamic shaker coupled with a Spektra VCS-201 controller to maintain the desired acceleration level. Frequency sweeps are performed at five RMS acceleration levels including 0.03 g, 0.05 g, 0.1 g, 0.3 g, and 0.5 g. Once the experimental voltage output is obtained for multiple acceleration levels and load resistances equal to R = 1 kΩ, 5 kΩ, 10 kΩ, 50 kΩ, 100 kΩ, and 500 kΩ, the nonlinear parameters are extracted by fitting the numerical voltage–frequency response curves with the corresponding experimental results. The experimental setup as well as the bimorph cross-section and sample voltage sweep results for a load resistance of R = 100 kΩ with the fitting are shown in Fig. 3.

The geometrical and physical quantities of the bimorph are listed in Table 1. All the identified parameters are in agreement with those identified by Leadenham and Erturk for the same beam, [25] except for the linear and nonlinear damping which can be attributed to minor differences in clamping and environmental conditions. It is also interesting to observe the behavior of the backbone curve for different load resistors. In Fig. 4, the experimental FRFs of voltage indicate that for increasing load resistance, the backbone curve remains linear but undergoes a clockwise rotation, limiting the effect of inherent nonlinearity (i.e. slight shift of the resonant frequency).

3. Experimental investigation and simulation

3.1. Setup description

The experimental procedure for studying the magnetic plucking has been realized with the setup showed in Fig. 5. The setup features a long stroke shaker (APS-113) with a magnet attachment. The shaker is actuated using a harmonic function with constant frequency of 3 Hz. The velocity of the moving magnet is measured using a laser Doppler Vibrometer (Polytec PDV-100), which is also used as the feedback signal for the vibration controller Spektra VCS-201 that maintains a specified maximum velocity level between 0.3 m/s and 0.7 m/s. The voltage output of the bimorph is measured across a load resistor ranging from 1 kΩ up to 100 MΩ, while the tip velocity is recorded with a Polytec OFV-505 vibrometer. A linear precision positioner is used to accurately set the gap distance between the magnets with little uncertainty (±0.025 mm) by moving the clamped bimorph.

Table 1
Physical and geometrical data of the piezoelectric bimorph.

Description	Symbol	Value	Unit
Total beam length	L^*	31.8	mm
Overhang length	L	26.7	mm
Width	b	3.16	mm
PZT-5A layer thickness	h_p	0.265	mm
Brass layer thickness	h_b	0.125	mm
PZT-5A mass density	ρ_p	7800	kg/m^3
PZT-5A Young's modulus[a]	$c_{11,p}$	66	GPa
PZT-5A nonlinear elastic constant	$c_{111,p}$	−60	TPa
PZT-5A linear piezoelectric constant[a]	e_{31}	−11.6	C/m^2
PZT-5A nonlinear piezoelectric constant	e_{311}	−20	kC/m^2
PZT-5A dielectric constant	ε_{33}	14.6	nF/m
Brass mass density	ρ_b	8500	kg/m^3
Brass Young's modulus	$c_{11,s}$	100	GPa
Linear damping coefficient[b]	b_1	1.70e1	N/m
Nonlinear damping coefficient[b]	b_2	9.00e5	N/m^2

[a] Constants provided by the supplier.

[b] These values are obtained by direct fitting on the lumped-parameter model of the Eq. (4).

The relative velocity of interaction is manipulated by acting only on the amplitude of the signal provided to the shaker. The system is built in such a way that the peak velocity of the input harmonic signal occurs at the minimum distance between the magnets (i.e. h in Fig. 1). The magnets are in the repulsive configuration, that is of most interest for energy harvesting [16]. It is important to underline that, in general, it is not necessary for the moving magnet to follow a harmonic motion for having plucking [30]. In any case, the impulsive character of the magnetic interaction is connected to the relative velocity rather than to the amplitude of the movement of the moving magnet.

3.2. Effect of the plucking velocity

The first investigation concerns the observation of voltage–time histories for a fixed gap distance h = 2.5 mm between the magnets and for a fixed electrical resistance R = 100 kΩ, and varying velocities of the magnetic interaction. Fig. 6 shows the recordings made for the different tests. For the slower case (0.3 m/s, top left), it can be observed that there is a snap in tension experienced by the bimorph but there is no presence of high-frequency vibration. This is due to the fact that the observed phenomenon is basically quasi-static and corresponds to the deflection and discharge of the beam under the action of the magnetic force. By considering the increasing velocity, as indicated in the other plots of Fig. 6, gradually the presence of the free-vibration of the bending mode appears. In the case of 0.4 m/s, a weak presence of the first mode is observed after the voltage peaks. In that case, the beam attempts to vibrate but the moving magnet attached to the shaker is still close enough to interact and suppress the oscillation. As the velocity increases, the moving magnet is gradually further away from the beam. The magnetic interaction after the peak is in that case always lower, allowing the beam to oscillate more and more tending towards the free vibration condition. An increase in the interaction velocity has a clear effect on the impulsiveness of the induced magnetic force. For the 0.3 m/s case, it is observed in the plots that the induced quasi-static phenomenon lasts about 0.05 s. For the faster case (0.7 m/s), the snap phase preceding the high-frequency vibration lasts about 0.017 s. The impulsiveness of the phenomenon also has an effect in terms of signal magnitude which increases as the velocity increases. This is due to a completely different dynamics as the initial velocity conditions of the beam change. The inertial effects are also gradually different. In fact, the positional nature of the force imposes that the beam must always reach the same maximum deflection during the magnetic interaction phase. However, for increasing velocities, the beam will have less and less time to reach that spatial configuration, experiencing not only speeds but also different accelerations, and so inertial effects.

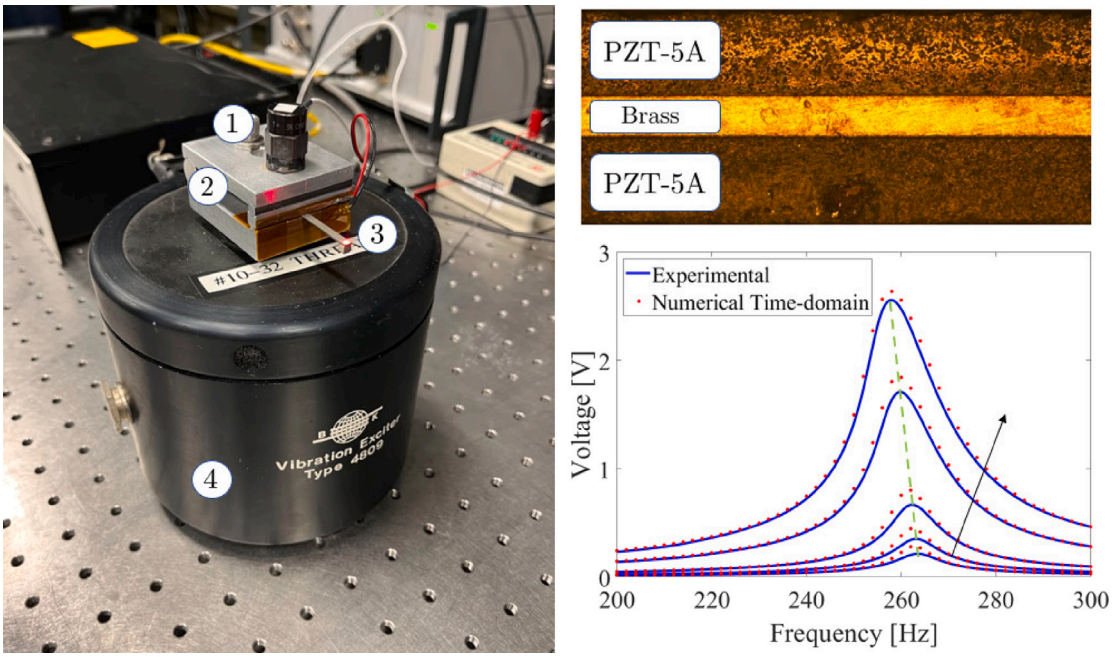

Fig. 3. *Left*: experimental apparatus used for the sweeps including (1) accelerometer, (2) clamp, (3) cantilever with a tip magnet, and (4) shaker. *Top right*: cross section of the bimorph, obtained from [29]. *Bottom right*: comparison of voltage–frequency plots between experimental results and numerical time-domain analysis with $R = 100$ kΩ using the fitted nonlinear parameters. The arrow indicates increasing amplitude of RMS acceleration.

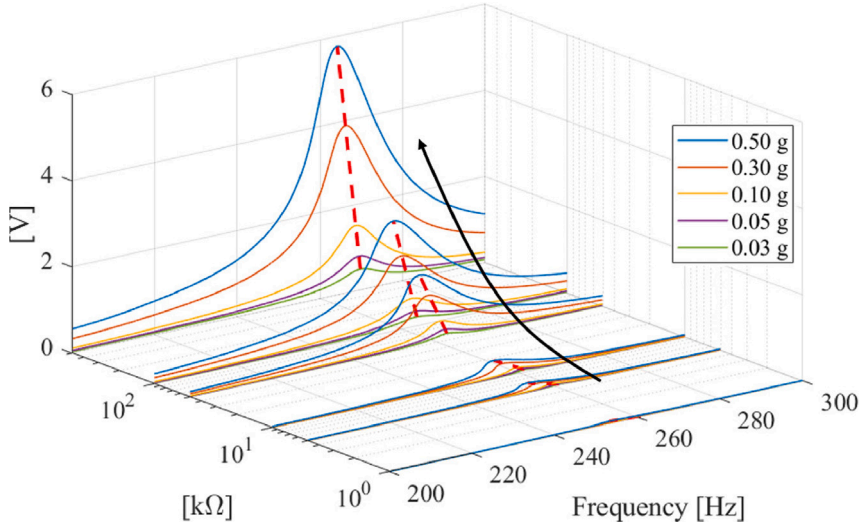

Fig. 4. FRFs of voltage of the cantilever without tip mass for different RMS acceleration levels including 0.03 g, 0.05 g, 0.1 g, 0.3 g, and 0.5 g, and load resistance between 1 kΩ and 500 kΩ.

3.3. Frequency content migration and inherent nonlinearities

Further considerations on the plucking mechanism can be made by considering the frequency response of the bimorph. In particular, it is observed how frequency migration (from low to high frequency) occurs through the voltage response, by considering just a single magnetic plucking cycle which consists of magnetic interaction between the magnets and a possible subsequent high-frequency free vibration. It is considered the influence of various parameters which are described below. To conduct such observation, fast Fourier transforms (FFTs) are observed. Fig. 7 (left), shows the FFT of the voltage response as the gap between the magnets changes, with the same chosen load resistance and interaction velocity fixed at 0.7 m/s. As can be seen, an increase in the gap distance between the magnets lowers the amplitudes. This can be explained by considering that as the gap distance increases, the magnetic force decreases, limiting the deflection experienced by the beam which have a direct consequence on the voltage amplitudes. Two peaks are observed in the FFTs: one at low frequency, between 25 Hz and 70 Hz associated with the magnetic force exchanged between the magnets, and another one around 260 Hz which is associated with the first bending mode of the bimorph. As will be seen later in detail, the frequency associated with this mode can slightly change due to inherent nonlinearities. In general, however, the presence of the second peak in the FFTs is not guaranteed. The fact is due to the activation of free vibrations of the cantilever only if the relative velocity is large enough, as explained in Section 3.2. As shown in the voltage–time histories of Fig. 6, the phenomenon must be fast enough for the same frequency of the input signal to induce vibration. If the velocity at which the magnets interact is not high enough, there is no high-frequency oscillation (see the case with 0.3 m/s in Fig. 6) and the highest frequency peak would

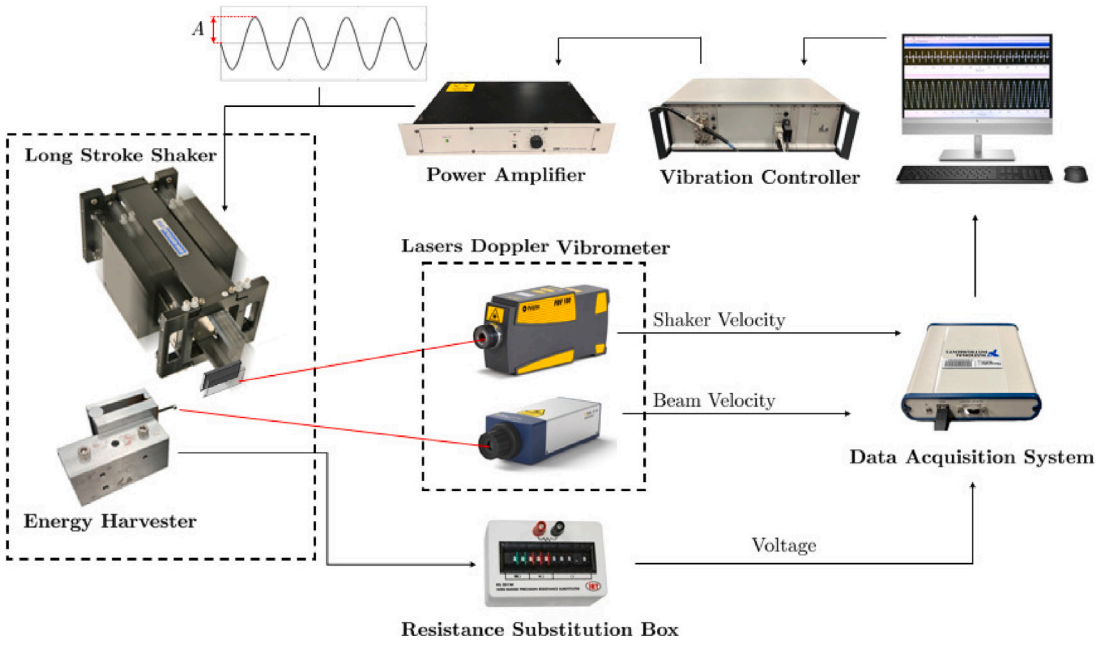

Fig. 5. Frequency up-conversion experimental apparatus.

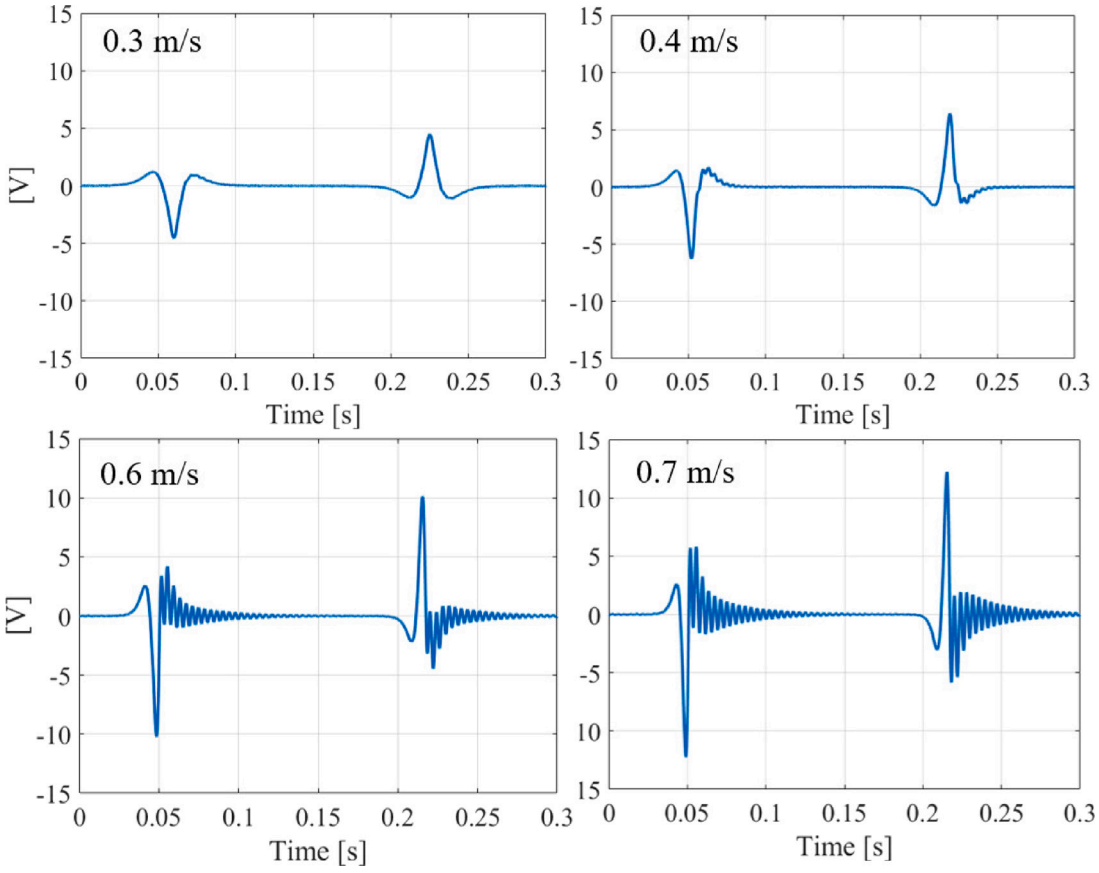

Fig. 6. Experimental voltage–time histories for varying velocities of interaction (0.3 m/s, 0.4 m/s, 0.6 m/s, 0.7 m/s), gap distance h = 2.5 mm, R = 100 kΩ.

disappear. Such observation is confirmed by the plot of Fig. 7 (right) in which the FFTs of different recordings are represented for a fixed gap distance of 2.5 mm, a resistor of 100 kΩ and variable velocity in the range 0.3 m/s–0.7 m/s. For the case of 0.3 m/s, there is the exclusive presence of a single peak at 24.94 Hz. By increasing the velocity of the shaker, with the same frequency of 3 Hz, the second peak gradually appears and is always higher in frequency. Thus the positional nature of the magnetic force means that frequency conversion of an input signal to the structural mode of interest may or may not occur, at a given input frequency. What therefore determines the success of the frequency up-conversion is a sufficiently fast interaction between the magnets. This is due to the fact that the initial conditions of displacement and velocity

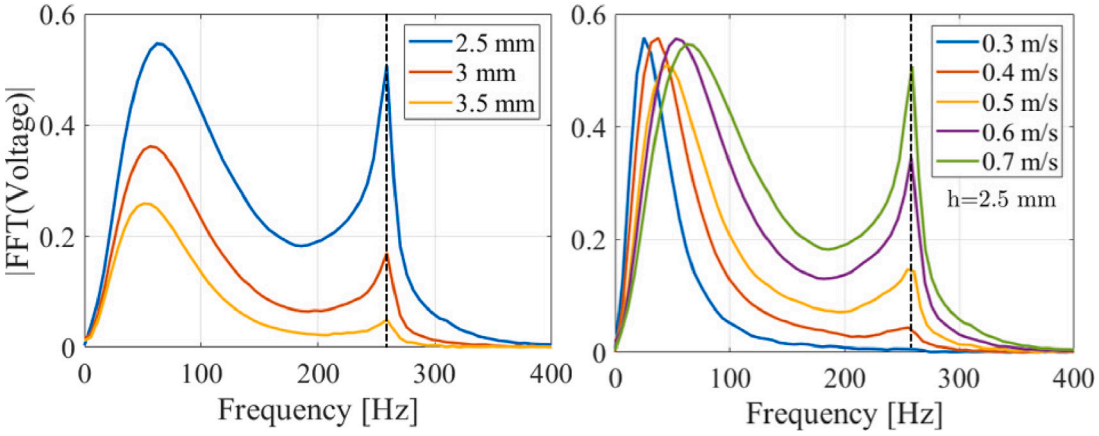

Fig. 7. Experimental voltage FFTs for different gap distances h with a velocity of interaction equal to 0.7 m/s, R = 100 kΩ (left). FFTs for varying velocities of interaction and gap distance h = 2.5 mm (right). The black dashed line identifies the frequency of the first bending mode of the bimorph.

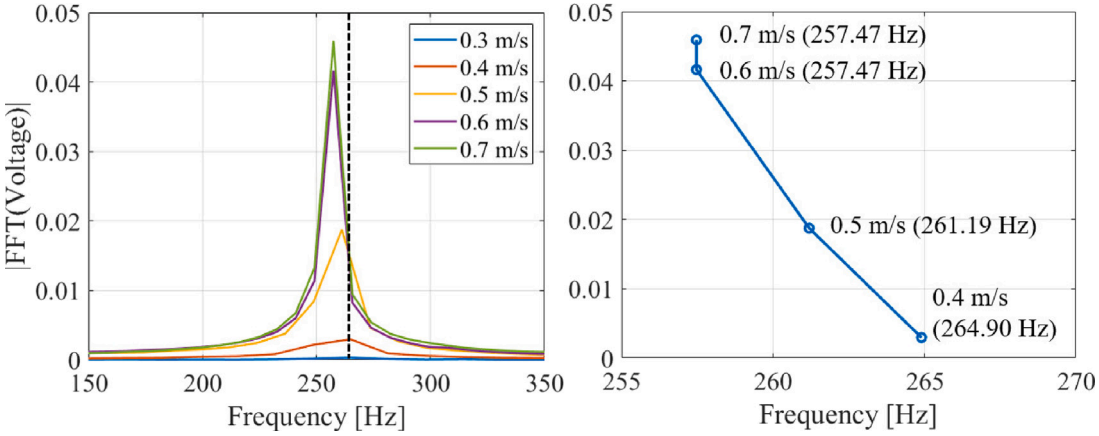

Fig. 8. Experimental voltage FFTs for varying velocities of interaction, gap distance h = 2.5 mm, R = 5 kΩ (left). Zoom on the peaks of the FFTs for varying velocities of interaction and gap distance h = 2.5 mm (right).

determine different dynamics in a mechanical system. Also, the higher velocity of the moving magnet means that after the first snap of the beam, there is more space to oscillate without interference with the repulsive magnetic interaction. In Fig. 7 (right) it is detected also a gradual shift of the first peaks to higher frequencies for the increasing velocity of the shaker. This is due to the more rapid interaction between the magnets.

The frequency shift effect due to the increase in load resistance is a well-known behavior in piezoelectric vibration energy harvesting systems [8] in conditions of harmonic motion of the support. In a more general context in terms of material behavior, the frequency sweep of the plot in Fig. 4 for different accelerations amplitudes and resistance showed both the effect of frequency shift due to electromechanical coupling and also greater inherent material nonlinearity (softening), as the short circuit condition is approached. This can be clearly seen by looking at the various inclination of the backbone curves (dashed red curves) which tend to vertical for increasing electrical resistance. The latter fact can be seen as a stiffening effect provided by increasing the load resistance. The presence of inherent material nonlinearity has been also observed in the plucking phenomenon, especially near the short circuit condition. In fact, Fig. 8 shows that by using in the experiment R = 5 kΩ and focusing only on the high-frequency phase of the beam (i.e. by excluding the first peak in the FFTs), for increasing velocity of interaction, a shift to lower frequencies of the first bending mode of the beam is detected. In more detail, Fig. 8 (left) shows the FFTs, and 8 (right) the zoomed view of the peaks for velocities that include the activation of the first mode. This means that the beam is losing stiffness and this is attributable to inherent material nonlinearities, having excluded geometric-type nonlinearities (very stiff cantilever). Furthermore, the experienced electric field values are well below the coercive field of the piezoelectric material and so, dielectric or ferroelectric nonlinearities are here excluded. The observed nonlinearities are of the ferroelastic type [25]. Such phenomenon implies that if the natural frequency of the resonator changes, also the optimal condition for energy harvesting will change. In the same plot, it can be seen that in the cases of 0.6 m/s and 0.7 m/s, the oscillator exhibits the peak at the same frequency of 257.47 Hz. This is attributable to the fact that the amplitude of the measured signal changes little from 0.6 m/s to 0.7 m/s. Furthermore, it is observed in the time histories of Fig. 6 that between 0.4 m/s and 0.6 m/s, the system radically changes its dynamics from a “no plucking” to a “plucking” state. The amplitude of the signal is therefore not proportional to the velocity of the shaker, since different dynamics can be activated.

Another observation is the fact that in the experimental mechanism of this work, the imposed velocities experienced by the moving magnet are guaranteed since it is externally driven. In other words, the magnetic interaction does not influence the motion law of the shaker. In more practical and realistic cases [16] this cannot be guaranteed, because the magnetic force is often two-way coupled and can influence the dynamics of the moving magnet. In that case, considering the repulsive configuration, this influence is not known a priori which depends case by case on the characteristics of the involved resonators.

Experimental parametric analyses have been conducted by considering velocities and load resistances in the range 0.3 m/s–0.7 m/s and

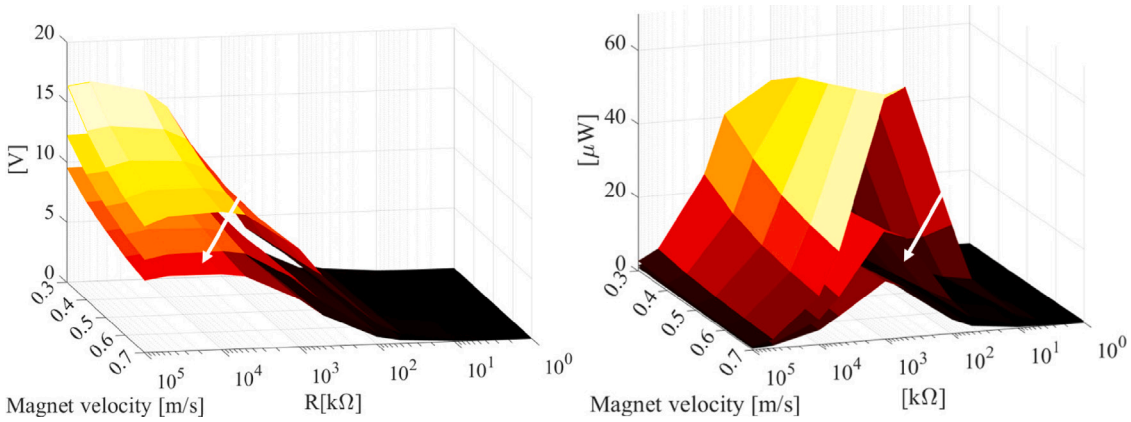

Fig. 9. Experimental parametric analyses for the RMS voltage over 2.5 s (left) and the associated power (right) for varying electrical load resistor R, and velocity of the magnetic interaction. The arrow indicates increasing gap distance h (2.5 mm, 3.0 mm, 3.5 mm).

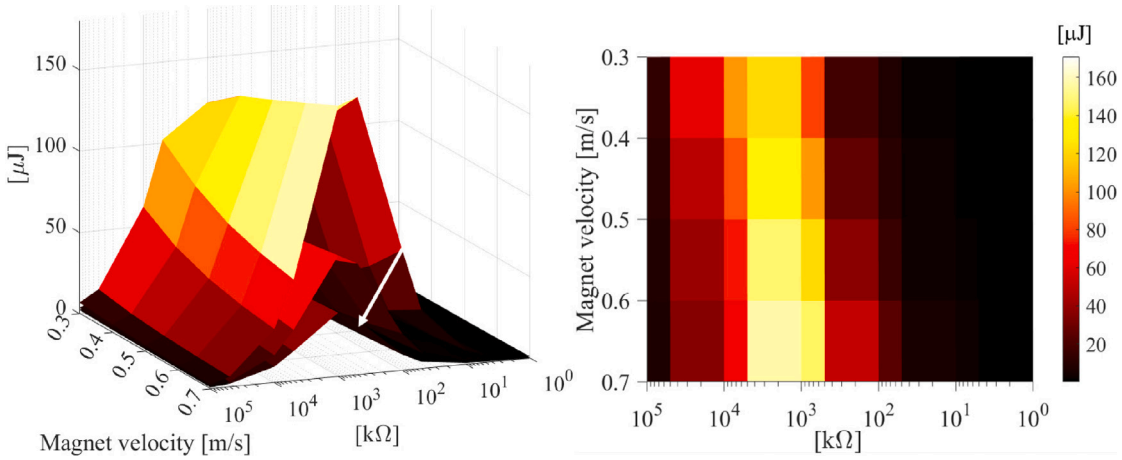

Fig. 10. Experimental parametric analyses for energy over 2.5 s of test, the arrow indicates increasing gap distance h (2.5 mm, 3.0 mm, 3.5 mm), (left). Top view for the case of gap h = 2.5 mm (right).

1 kΩ–100 MΩ, respectively. Three values of gap distance have been considered: h = 2.5 mm, 3.0 mm, and 3.5 mm. The results are plotted in Fig. 9 for the RMS voltage (left) and the associated power dissipated in the resistor (right), through the Joule's Law:

$$P = \frac{V_{RMS}^2}{R} \tag{6}$$

where V_{RMS} is the RMS voltage and R the electrical resistance. In the aforementioned plots, different surfaces correspond to different gap distances. By increasing the gap distance between the magnets (indicated by black arrow in the plots) the output voltage decreases. This is reasonable considering that the magnetic force also decreases.

The plot in Fig. 10 (left) shows the trend of the energy obtained in the tests over 2.5 s of operation. Again, different surfaces indicate different gap distance h. In all cases, the optimal load is identified around 1 MΩ, except for the case with a smaller gap distance, h = 2.5 mm. In this case, the optimal load shift could be attributed to the inherent nonlinearities since the force values are higher than in the other cases and the phenomenon is the fastest among the considered ones. Fig. 10 (right) shows the plot of the energy from the top and it can be appreciated that depends on the optimal conditions. For low velocity values (e.g. 0.3 m/s), a significant band of obtainable energy is between 1–5 MΩ, if instead the velocity increases, the highest values of the considered surface (therefore gap) tend to gather between 0.5–1 MΩ. The same behavior is exhibited for the other considered gap distances.

3.4. Numerical time-domain simulation — comparison with experimental results

The calibration of the computational model (4) allows to perform time-domain numerical simulation. A MATLAB program has been developed that solves the system of ODEs with the Runge–Kutta method. For the case of R = 100 kΩ and h = 2.5 mm, Fig. 11 shows the comparison between the experimental and the numerical response over 2 s, in which the nonlinear terms in the differential system (4) have been neglected. The plot in Fig. 12 instead, shows the comparison taking into account inherent nonlinearities (stiffness, ferroelastic hysteresis, and coupling). The plots in Fig. 13 show that the model manages with excellent approximation to capture the response also for other resistor values (left) and velocities of interaction (right). The simulation results show that in harvesters subjected to magnetic interaction, strain values can be such to compromise the validity of the linear piezoelectricity hypothesis. By considering reversible (elasticity and coupling) and nonconservative (damping) nonlinearities sources the prediction of the behavior can be improved.

4. Conclusions

In this work, the dynamical behavior of a frequency up-converted piezoelectric energy harvester is investigated by means of magnetic forces between permanent magnets. The experiments showed that at a fixed low frequency of 3 Hz the FuC occurs only for sufficiently high velocities from 0.4 m/s to 0.7 m/s. The results of this aspect of the

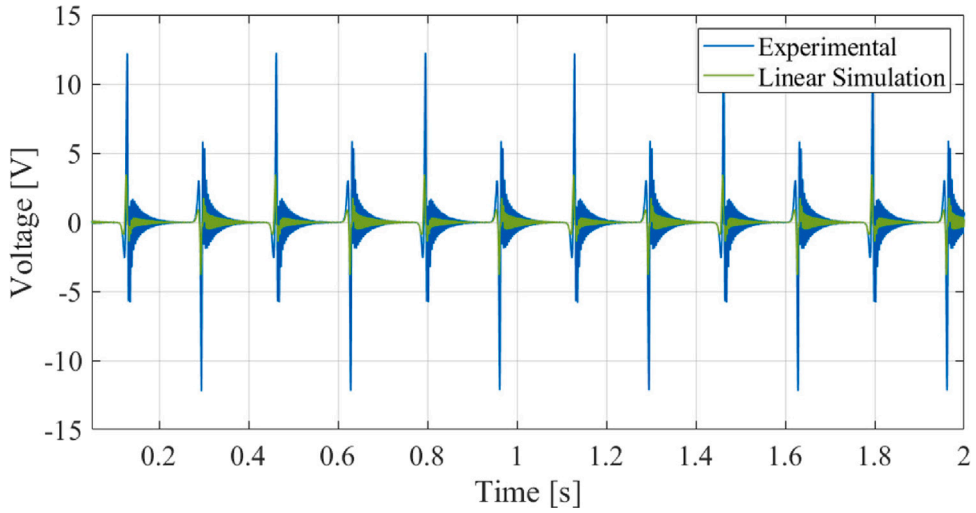

Fig. 11. Comparison between experimental response and time-domain numerical simulation performed with linear piezoelectricity, gap distance h = 2.5 mm, R = 100 kΩ, and velocity of interaction 0.7 m/s over 2 s.

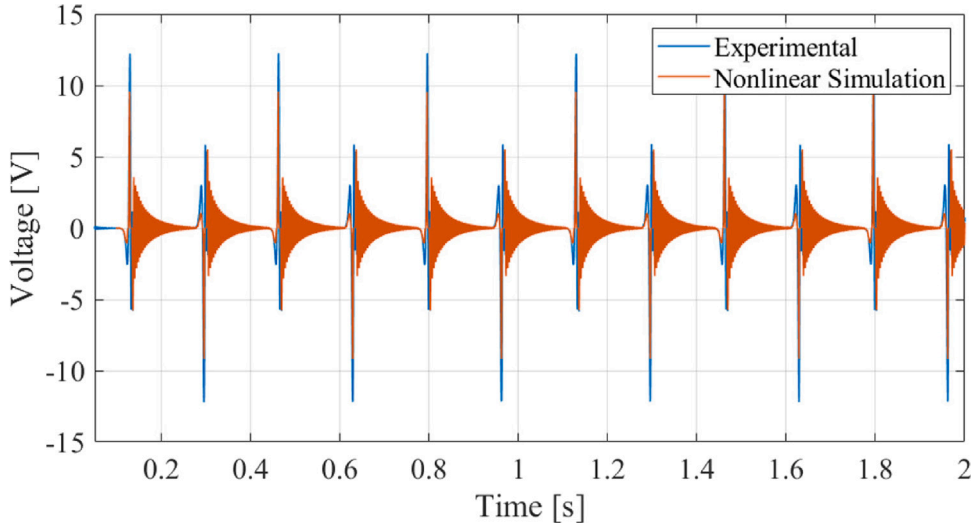

Fig. 12. Comparison between experimental response and time-domain numerical simulation performed with the nonlinear electroelastic model, gap distance h = 2.5 mm, R = 100 kΩ, and velocity of interaction 0.7 m/s over 2 s.

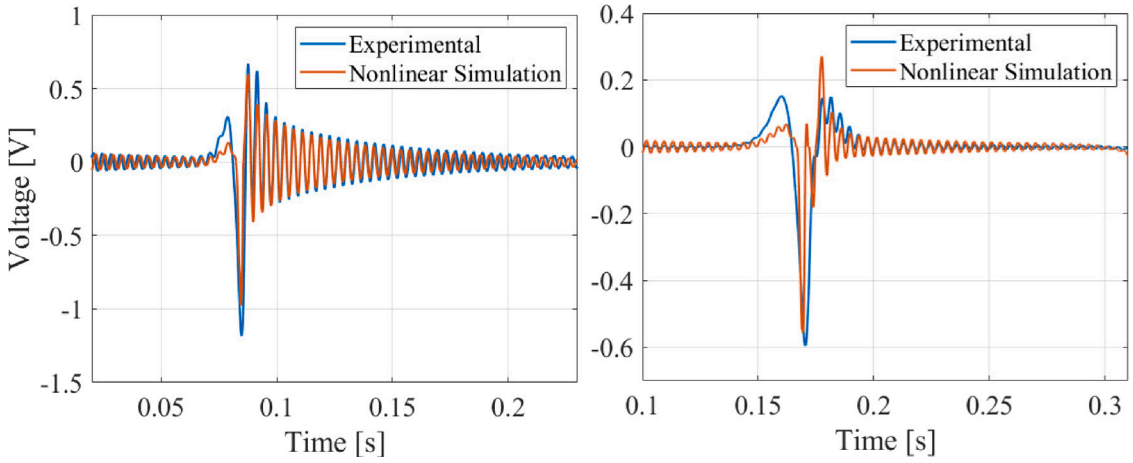

Fig. 13. Zoom on a single plucking and free-vibration phase, h = 2.5 mm, R = 10 kΩ. Comparison between experiments and nonlinear electroelastic time-domain simulation with velocity of the moving magnet equal to 0.7 m/s (left), and 0.4 m/s (right).

work show that the design of a magnetic FuC mechanism is strictly linked to the expected operational speeds of the moving magnet. Such a fact leads primarily to the conclusion that the design phase requires knowing the velocities to which the device will be subjected. Hence the specific application field of the harvester beyond the frequency content of the seismic signal should be considered. For the sake of completeness, it is emphasized that in a real device, the dynamic behavior could get even more complicated. In the studied system, the seismic mass (i.e. the shaker) is externally driven and therefore the interaction velocity values are guaranteed and coincide with the input ones. In a real object, the magnetic interaction could be such as to influence the velocity values of the seismic mass, thus slowing down the phenomenon in the repulsive case. In general, this does not happen when the kinetic energy of the seismic mass is much greater than the work done by the magnetic force along the interaction path. It has also been observed that the peak velocity of the transducer is always lower than those provided by the moving magnet input and this value varies significantly even with the considered resistor and gap distance between magnets.

Furthermore, another novel contribution is that the presence of softening has been observed, which leads to variations in the dynamic characteristics. This aspect should not be neglected in a conscious design of the plucking mechanism, especially when the gap between the magnets is very low and the resulting forces are high. The softening phenomenon can be captured with sufficient accuracy by a lumped parameter mathematical model if also the material inherent nonlinearities (elasticity, coupling, and ferroelastic effects) are considered. Obviously, the sources of nonlinearity to be considered can change in a different context, such as dielectric effects and/or nonlinear kinematics. The drawback of using a nonlinear model is the fact that a specific calibration is needed, and usually, the data sheets for transducers do not provide a nonlinear mechanical characterization. The effort could be avoided on the industrial scale, where processes benefit from repeatability and a single characterization is valid for a large number of devices.

The limitation of the magnetic FuC related to the velocity of the interacting objects opens new perspectives in terms of strategies to design FuC systems when the velocity of the input signal is not sufficient to trigger the harvester. A possible solution could be to combine the magnetic interaction with multistable systems able to accumulate potential energy and release it suddenly in terms of kinetic energy to increase the velocity of the interaction.

CRediT authorship contribution statement

Michele Rosso: Conceptualization, Methodology, Software, Validation, Formal analysis, Investigation, Data curation, Writing – original draft, Writing – review & editing, Visualization. **Eetu Kohtanen:** Conceptualization, Methodology, Validation, Investigation, Writing – original draft, Writing – review & editing. **Alberto Corigliano:** Conceptualization, Methodology, Writing – original draft, Writing – review & editing. **Raffaele Ardito:** Conceptualization, Methodology, Resources, Writing – original draft, Writing – review & editing, Supervision. **Alper Erturk:** Conceptualization, Methodology, Resources, Writing – original draft, Writing – review & editing, Supervision.

Declaration of competing interest

The authors declare that they have no known competing financial interests or personal relationships that could have appeared to influence the work reported in this paper.

Data availability

Data will be made available on request.

Acknowledgments

MR wish to thank Prof. Alper Erturk for being hosted at Georgia Institute of Technology (Atlanta, USA) and for the opportunity to have worked with his group at the Smart Structures and Dynamical Systems Lab (SSDSL).
MR wish to thank Prof. Stefano Lenci for a fruitful discussion on the backbone curves.
RA, AC, and MR acknowledge the support of the European Union, through the H2020 FET-proactive project MetaVEH, grant agreement No. 952039.

Appendix A. Mathematical model of the bimorph

Kinetic energy. The kinetic energy $\mathcal{K}$ of the system is the sum of the contributions of the beam and of the tip mass:

$$\mathcal{K} = \mathcal{K}_b + \mathcal{K}_t \tag{A.1}$$

The kinetic energy of the piezoelectric beam is:

$$\mathcal{K}_b = \frac{1}{2}\int_0^L b\, m_d \left[\left(\frac{\partial u_3}{\partial t}\right) + \left(\frac{\partial y}{\partial t}\right)\right]^2 dx_1 \tag{A.2}$$

In Eq. (A.2) the mass density for unit length of the layered beam has been introduced m_d:

$$m_d = \sum_{k=1}^{N}\int_{x_{3,k-1}}^{x_{3,k}} \rho^k\, dx_3 \tag{A.3}$$

where ρ^k is the mass density of the kth layer. Since the beam is supposed very thin, its rotational inertia terms have been neglected. In the following, the distributed mass $\hat{m}$ will be used:

$$\hat{m} = b\left(\rho_s h_s + 2\rho_p h_p\right) \tag{A.4}$$

where ρ_s, ρ_p are the mass densities and h_s, h_p the thicknesses of the structural and the piezoelectric layers. The kinetic energy of the tip mass can be computed as:

$$\begin{aligned}\mathcal{K}_t =& \frac{1}{2}\left[m_t\left(\frac{\partial u_3}{\partial t}\right)^2 + J_t\left(\frac{\partial^2 u_3}{\partial t \partial x_1}\right)^2 + 2S_t\left(\frac{\partial u_3}{\partial t}\right)\left(\frac{\partial^2 u_3}{\partial t \partial x_1}\right)\right.\\ &\left. + m_t\left(\frac{\partial y}{\partial t}\right)^2\right]_{x_1=L} + \frac{\partial y}{\partial t}\left(m_t\frac{\partial u_3}{\partial t} + S_t\frac{\partial^2 u_3}{\partial t \partial x_1}\right)_{x_1=L}\end{aligned} \tag{A.5}$$

where m_t, J_t, S_t, are respectively the tip mass, its second order moment with respect the neutral axis of the beam and the first order moment. The presence of the first order moment in Eq. (A.5) is due to the asymmetry of the tip mass with respect to the longitudinal axis of the beam. The vertical motion of the support has been called y.

Internal energy.

$$\mathcal{E} = \int_{\mathcal{V}_s} H_s\, d\mathcal{V} + \int_{\mathcal{V}_p} H_p\, d\mathcal{V} \tag{A.6}$$

where H_s is the enthalpy of the structural layer and H_p of the piezoelectric Layer, and $\mathcal{V}_s$ and $\mathcal{V}_p$ are the volume of the structural and piezoelectric layer, respectively. For the structural layer, only linear elasticity is assumed. i.e.:

$$H_s = \frac{1}{2}c_{11,s}S_1^2 \tag{A.7}$$

Developing the integral (A.6), it is possible to write:

$$\begin{aligned}\mathcal{E} = \int_0^L \left\{\hat{k}_1\left(\frac{\partial^2 u_3}{\partial x_1^2}\right)^2 + \frac{1}{3}\hat{k}_2\left(\frac{\partial^2 u_3}{\partial x_1^2}\right)^3 \operatorname{sgn}\left(\frac{\partial^2 u_3}{\partial x_1^2}\right) - \left[2\hat{\theta}_1\frac{\partial^2 u_3}{\partial x_1^2} + \right.\right.\\ \left.\left. + \hat{\theta}_2\left(\frac{\partial^2 u_3}{\partial x_1^2}\right)^2 \operatorname{sgn}\left(\frac{\partial^2 u_3}{\partial x_1^2}\right)\right] v\right\} dx_1 - \frac{1}{2}Cv^2\end{aligned} \tag{A.8}$$

where the coefficients in Eq. (A.8) are defined below. $\hat{k}_1$ is the distributed linear stiffness:

$$\hat{k}_1 = \frac{1}{12}c_{11,s}bh_s + \frac{1}{6}c_{11,p}bh_p\left(4h_p^2 + 6h_ph_s + 3h_s^2\right) \tag{A.9}$$

and $\hat{k}_2$ is the distributed nonlinear stiffness:

$$\hat{k}_2 = \frac{1}{2}c_{111,p}bh_p\left(2h_p^3 + 4h_p^2h_s + 3h_ph_s^2 + h_s^3\right) \tag{A.10}$$

In Eq. (A.10) the nonlinear contribution is only provided by the piezoelectric material through the coefficient $c_{111,p}$. In the case of a series connection of electrodes of the layers, the distributed linear and nonlinear electromechanical coefficients $\hat{\theta}_1$ and $\hat{\theta}_2$ are respectively:

$$\hat{\theta}_1 = \frac{1}{2}e_{31}b\left(h_p + h_s\right) \tag{A.11}$$

$$\hat{\theta}_2 = \frac{1}{12}e_{311}b\left(4h_p^2 + 6h_ph_s + 3h_s^2\right) \tag{A.12}$$

The internal capacitance is:

$$C = \frac{bL^*\varepsilon_{33}}{2h_p} \tag{A.13}$$

where L^* is the effective total length of the beam. The overhanging cantilever length L is lower than L^* because a small portion of the length must be inserted among suitable plates to realize the clamp.

Coefficients of the equations of motion. By applying Hamilton's principle in the form:

$$\int_{t_0}^{t_1}\left(\delta\mathcal{L} + \delta W_{nc}\right)\,dt = 0 \tag{A.14}$$

it is possible to derive the system of nonlinear ODEs (4). In Eq. (A.14), $\mathcal{L}$ is the Lagrangian function which is defined as the difference between the kinetic and the total potential energy $\mathcal{U}$. The total potential energy is then defined as the difference between the internal energy $\mathcal{E}$ and the external work $\mathcal{W}$. The nonconservative virtual work δW_{nc} is assumed equal to [25]:

$$\delta W_{nc} = -\int_0^L\left[\hat{b}_1u_3\,\mathrm{sgn}(u_3) + \hat{b}_2u_3^2\right]\mathrm{sgn}(\dot{u}_3)\delta u_3\,dx - \frac{v}{R}\delta\lambda \tag{A.15}$$

where λ is the flux linkage coordinate. Details on the mathematical derivation are extensively reported in [25]. According to the Euler–Bernoulli beam theory, the axial deformation is:

$$S_1 = -x_3u_3''(x_1,t) \tag{A.16}$$

where u_3 is the displacement of the beam in the orthogonal direction with respect to its axis x_1 (see Fig. 1). $()'$ means partial derivative with respect to x_1. The Galerkin's discretization with one dof is:

$$u_3(x_1,t) = \phi(x_1)u(t) \tag{A.17}$$

where the tip displacement of the cantilever $u(t)$ is the Lagrangian coordinate (or dof), and $\phi(x_1)$ is the first mode shape of a purely mechanical Euler–Bernoulli cantilever beam [25]. where the shape function of the Euler–Bernoulli beam $\phi(x_1)$ is:

$$\phi(x_1) = \frac{1}{2}\left\{\cosh\left(\frac{\beta x_1}{l}\right) - \cos\left(\frac{\beta x_1}{l}\right) - \sigma\left[\sinh\left(\frac{\beta x_1}{l}\right) - \sin\left(\frac{\beta x_1}{l}\right)\right]\right\} \tag{A.18}$$

with $\beta = 1.8751$ and $\sigma = 0.7341$. The model for the electric field E_3, that has been assumed in case of series connection of the piezoelectric layer [8] is:

$$E_3 = -\frac{v}{2h_p} \tag{A.19}$$

where h_p is the thickness of the piezoelectric layer, and v is the voltage across the electrodes. The computed coefficients for the equations of motions are the following:

$$m = \hat{m}\int_0^L\phi^2\,dx_1 \tag{A.20}$$

$$b_1 = \hat{b}_1\int_0^L\phi^2\,dx_1 \tag{A.21}$$

$$b_2 = \hat{b}_2\int_0^L\phi^3\,\mathrm{sgn}\left(\phi\right)\,dx_1 \tag{A.22}$$

$$k_1 = \hat{k}_1\int_0^L\frac{\partial^4\phi}{\partial x_1^4}\phi\,dx_1 \tag{A.23}$$

$$k_2 = \hat{k}_2\int_0^L\left[\frac{\partial^2\phi}{\partial x_1^2}\frac{\partial^4\phi}{\partial x_1^4} + \left(\frac{\partial^3\phi}{\partial x_1^3}\right)^2\right]\phi\,\mathrm{sgn}\left(\frac{\partial^2\phi}{\partial x_1^2}\right)dx_1 \tag{A.24}$$

$$\theta_1 = \hat{\theta}_1\left(\frac{\partial\phi}{\partial x_1}\right)_{x_1=L} \tag{A.25}$$

$$\theta_2 = \hat{\theta}_2\int_0^L\frac{\partial^4\phi}{\partial x_1^4}\phi\,\mathrm{sgn}\left(\frac{\partial^2\phi}{\partial x_1^2}\right)dx_1 \tag{A.26}$$

Appendix B. Magnetic force

By considering Fig. 2, one Cartesian reference system is associated to each magnet. α, β and γ are the vector components of the distance between the centers O and O′ of the reference systems, and a, b, c, A, B, C are the half-lengths of the sides of the magnets. The coefficients that appear in Eq. (5) are the following:

$$\phi_x(U_{mn},V_{pq},W_{rs},R) = \frac{V_{pq}^2 - W_{rs}^2}{2}ln(R-U_{mn}) + U_{mn}V_{pq}ln(R-V_{pq}) + V_{pq}W_{rs}\arctan\left(\frac{U_{mn}V_{pq}}{W_{rs}R}\right) + \frac{1}{2}U_{mn}R \tag{B.1}$$

$$\phi_y(U_{mn},V_{pq},W_{rs},R) = \frac{U_{mn}^2 - W_{rs}^2}{2}ln(R-V_{pq}) + U_{mn}V_{pq}ln(R-U_{mn}) + U_{mn}W_{rs}\arctan\left(\frac{U_{mn}V_{pq}}{W_{rs}R}\right) + \frac{1}{2}V_{pq}R \tag{B.2}$$

$$\phi_z(U_{mn},V_{pq},W_{rs},R) = -U_{mn}W_{rs}ln(R-U_{mn}) - V_{pq}W_{rs}ln(R-V_{pq}) + U_{mn}V_{pq}\arctan\left(\frac{U_{mn}V_{pq}}{W_{rs}R}\right) - W_{rs}R \tag{B.3}$$

The coefficients U_{mn}, V_{pq}, W_{rs}, R that appear in Eqs. (B.1)–(B.3) are defined as:

$$U_{mn} = \alpha + A(-1)^n - a(-1)^m \tag{B.4}$$

$$V_{pq} = \beta + B(-1)^q - b(-1)^p \tag{B.5}$$

$$W_{rs} = \gamma + C(-1)^s - c(-1)^r \tag{B.6}$$

$$R = \sqrt{U_{mn}^2 + V_{pq}^2 + W_{rs}^2} \tag{B.7}$$

and they have dimensions of lengths.

References

[1] S.R. Anton, H.A. Sodano, A review of power harvesting using piezoelectric materials (2003–2006), Smart Mater. Struct. 16 (2007) R1–R21, http://dx.doi.org/10.1088/0964-1726/16/3/R01.

[2] M. Safaei, H.A. Sodano, S.R. Anton, A review of energy harvesting using piezoelectric materials: state-of-the-art a decade later (2008–2018), Smart Mater. Struct. 28 (62pp) (2019) 113001, http://dx.doi.org/10.1088/1361-665X/ab36e4.

[3] J. Yang, An Introduction To the Theory of Piezoelectricity, second ed., in: Advances in Mechanics and Mathematics Series, Springer Nature Switzerland AG, 2018.

[4] S. Trolier-McKinstry, P. Muralt, Thin film piezoelectrics for MEMS, J. Electroceram. 12 (2004) 7–17, http://dx.doi.org/10.1023/B:JECR.0000033998.72845.51.

[5] R. Ardito, E. Bertarelli, A. Corigliano, G. Gafforelli, On the application of piezolaminated composites to diaphragm micropumps, Compos. Struct. 99 (2013) 231–240.

[6] S. Roundy, P.K. Wright, J.M. Rabaey, Energy Scavenging for Wireless Sensor Networks, Springer, New York, 2004.
[7] S. Priya, D. Inman, Energy Harvesting Technologies, Springer, New York, 2009.
[8] A. Erturk, D.J. Inman, Piezoelectric Energy Harvesting, Wiley, Chichester, 2011.
[9] D. Briand, E. Yeatman, S. Roundy, Micro energy harvesting wiley-CH, 2015.
[10] M. Pozzi, M. Zhu, Characterization of a rotary piezoelectric energy harvester based on plucking excitation for knee-joint wearable applications, Smart Mater. Struct. 21 (2012) 055004.
[11] B. Kathpalia, D. Tan, I. Stern, A. Erturk, An experimentally validated model for geometrically nonlinear plucking-based frequency up-conversion in energy harvesting, Smart Mater. Struct. 27 (2018) 015024.
[12] W.J. Su, Impact-driven broadband piezoelectric energy harvesting using a two degrees-of-freedom structure, Microsyst. Technol. (2020) http://dx.doi.org/10.1007/s00542-019-04744-1.
[13] P. Aceti, M. Rosso, R. Ardito, N. Pienazza, A. Nastro, M. Baù, M. Ferrari, M. Rouvala, V. Ferrari, A. Corigliano, Optimization of an impact-based frequency up-converted piezoelectric vibration energy harvester for wearable devices, Sensors 23 (3) (2023) http://dx.doi.org/10.3390/s23031391.
[14] P. Pillatsch, B.L. Xiao, N. Shashoua, H.M. Gramling, E.M. Yeatman, P.K. Wright, Degradation of bimorph piezoelectric bending beams in energy harvesting applications, Smart Mater. Struct. 26 (10pp) (2017) 035046, http://dx.doi.org/10.1088/1361-665X/aa5a5d, (2017).
[15] Q.C. Tang, Y.L. Yang, X. Li, Bi-stable frequency up-conversion piezoelectric energy harvester driven by non-contact magnetic repulsion, Smart Mater. Struct. 20 (6pp) (2011) 125011.
[16] M. Rosso, A. Corigliano, R. Ardito, Numerical and experimental evaluation of the magnetic interaction for frequency up-conversion in piezoelectric vibration energy harvesters, Meccanica 57 (2022) 1139–1154, http://dx.doi.org/10.1007/s11012-022-01481-0.
[17] T.K. Chung, C.M. Wang, P.C. Yeh, T.W. Liu, C.Y. Tseng, C.C. Chen, A three-axial frequency-tunable piezoelectric energy harvester using a magnetic-force configuration, IEEE Sens. J. 14 (9) (2014) 3152–3163, http://dx.doi.org/10.1109/JSEN.2014.2325675.
[18] P. Pillatsch, E.M. Yeatman, A.S. Holmes, Magnetic plucking of piezoelectric beams for frequency up-converting energy harvesters, Smart Mater. Struct. 23 (12pp) (2014) 025009, http://dx.doi.org/10.1088/0964-1726/23/2/025009.
[19] P. Pillatsch, E. M.Yeatman, A. Holmes, A piezoelectric frequency up-converting energy harvester with rotating proof mass for human body applications, Sensors Actuators A 06 (2014) (2014) 178–185.
[20] H. Fu, E.M. Yeatman, Rotational energy harvesting using bi-stability and frequency up-conversion for low-power sensing applications: Theoretical modelling and experimental validation, Mech. Syst. Signal Process. 125 (2019) 229–244.
[21] Y.C. Shu, W.C. Wang, Y.P. Chang, Electrically rectified piezoelectric energy harvesting induced by rotary magnetic plucking, Smart Mater. Struct. 27 (11pp) (2018) 125006, http://dx.doi.org/10.1088/1361-665X/aae6ea.
[22] Y.C. Lo, C.C. Chen, Y.C. Shu, M.F. Lumentut, Broadband piezoelectric energy harvesting induced by mixed resonant modes under magnetic plucking, Smart Mater. Struct. 30 (12pp) (2021) 105026, http://dx.doi.org/10.1088/1361-665X/ac1d8f.
[23] T. Xue, S. Roundy, On the magnetic plucking configurations for frequency up-converting mechanical energy harvesters, Sensors Actuators A 253 (2017) 101–111.
[24] R. Dauksevicius, A. Kleiva, V. Grigaluinas, Analysis of magnetic plucking dynamics in a frequency up-converting piezoelectric energy harvester, Smart Mater. Struct. 27 (19pp) (2018) 085016, http://dx.doi.org/10.1088/1361-665X/aa8ad.
[25] S. Leadenham, A. Erturk, Unified nonlinear electroelastic dynamics of a bimorph piezoelectric cantilever for energy harvesting, sensing, and actuation, Nonlinear Dynam. 79 (2015) 1727–1743, http://dx.doi.org/10.1007/s11071-014-1770-x.
[26] F. Goldschmidtboeing, C. Eichhorn, M. Wischke, M. Kroener, P. Woias, The influence of ferroelastic hysteresis on mechanically excited PZT cantilever beams, in: Proceedings of the 11th International Workshop on Micro and Nanotechnology for Power Generation and Energy Conversion Applications, 2011, pp. 114–117.
[27] G. Akoun, J.P. Yonnet, 3D analytical calculation of the forces exerted between two cuboidal magnets, IEEE Trans. Magn. MAG-20 (5) (1984).
[28] S.C. Stanton, A. Erturk, B.P. Mann, D.J. Inman, Nonlinear piezoelectricity in electroelastic energy harvesters: Modeling and experimental identification, J. Appl. Phys. 108 (2010) 074903.
[29] S. Leadenham, Advanced Concepts in Nonlinear Piezoelectric Energy Harvesting: Intentionally Designed, Inherently Present, and Circuit Nonlinearities, Georgia Institute of Technology, Atlanta, United States of America, 2015.
[30] R. Ardito, M. Rosso, The effect of inherent nonlinearities in coupled piezo-magneto-electric vibration energy harvester, in: Proceedings of the X International Conference on Computational Methods for Coupled Problems in Science and Engineering, COUPLED PROBLEMS 2023, 2023, pp. 1–6.

Michele Rosso received his Ph.D. degree in Structural Engineering from Politecnico di Milano (Italy) in 2023, and is currently a Postdoctoral researcher at the Department of Civil and Environmental Engineering of the same university. His research interests are focused on vibration energy harvesting, multiphysics systems, linear and nonlinear structural dynamics. He is a member of AIMETA (Italian association of theoretical and applied mechanics), Euromech, and IEEE MEMS Technical community.

Eetu Kohtanen received the Ph.D. degree in mechanical engineering from the Georgia Institute of Technology (USA) in 2023 where he studied the structural dynamics of the human skull. He has published broadly in the domains of dynamics and acoustics including topics such as hydroelastic damping of structures subjected to uniform flow, vortex-induced piezoelectric energy harvesting, and transcranial radiation of leaky guided waves.

Alberto Corigliano Full professor of Solids and Structural Mechanics with the Department of Civil and Environmental Engineering of Politecnico di Milano, Italy. Member of the technical committee of Eurosime, Associate Editor of the European J. of Mechanics A/Solids, of Advanced Modeling and Simulation in Engineering Sciences and of Frontiers in Materials – Mechanics of materials. Bruno Finzi prize for Rational Mechanics of the "Istituto Lombardo Accademia di Scienze e Lettere" 2006, Euromech Fellow of the European Mechanics Society 2015, member of the "Istituto Lombardo Accademia di Scienze e Lettere" 2018. (Co) author of more than 330 papers, 13 patents, 2 books.

Raffaele Ardito is Associate Professor of Structural Mechanics at Politecnico di Milano, Department of Civil and Environmental Engineering. His research fields are theoretical, computational and experimental mechanics of Metamaterials, Smart Materials and Microsystems. His activity is focused on topics characterized by high interdisciplinarity, such as advanced functional materials (3D printing, piezoelectric, and magnetic materials), innovative structures (MEMS, metamaterials), structural monitoring and parametric identification. He is the coordinator of the research unit at Politecnico di Milano in the project MetaVEH, funded by Horizon2020. He is also author of several patents and co-founder of an industrial spin-off (Phononic Vibes).

Alper Erturk received the Ph.D. degree in engineering mechanics from Virginia Tech Blacksburg, USA, in 2009. He is currently Carl Ring Family Chair and Professor of Mechanical Engineering at Georgia Tech, Atlanta, USA, where he leads the Smart Structures and Dynamical Systems Laboratory. He has authored or coauthored two books and more than 250 papers on dynamics, vibration, and acoustics of passive and active structures. He is a fellow of the American Society of Mechanical Engineers (ASME) and the International Society for Optical Engineering (SPIE). He was a recipient of various awards. He is the Editor-in-Chief of Smart Materials and Structures journal.